Ceramics International 48 (2022) 24550–24559

Contents lists available at ScienceDirect

Ceramics International

journal homepage: www.elsevier.com/locate/ceramint

Sensitization effect of Nd^{3+} ions on Yb^{3+}/Nd^{3+} co-doped oxyfluoride glasses and study of their optical, fluorescence, and upconversion abilities for visible laser and NIR amplifier applications

G. Devarajulu [a], B. Kiran Kumar [b,c], P. Reddi Babu [b], M. Dhananjaya [b], Na-hyun Bak [a], Kedhareswara Sairam Pasupuleti [a], B. Deva Prasad Raju [b,*], Moon-Deock Kim [a,d,**]

[a] Department of Physics, Chungnam National University, 99Daehak-ro, Yuseong-gu, Daejeon, 34134, South Korea
[b] Department of Physics, Sri Venkateswara University, Tirupati, 517 502, India
[c] Department of Physics, Government Degree College, Rayachoty, 516269, India
[d] Institute of Quantum Systems (IQS), Chungnam National University, 99Daehak-ro, Yuseong-gu, Daejeon, 34134, South Korea

ARTICLE INFO

Keywords:
Oxyfluoride glasses
Nd^{3+} and Yb^{3+} ions
NIR fluorescence
Energy transfer
Gain cross-section
Upconversion

ABSTRACT

The development of laser technology has created intense demand for optical confinement materials with high performance. Herein the authors have been investigated Yb^{3+}-singly doped and Yb^{3+}/Nd^{3+}-codoped SiO_2-based oxyfluoride glasses in terms of their optical absorption, and their near-infrared (NIR) and up-conversion (UC) emissions including emission decay profiles. Under 808 nm laser diode (LD) excitation, four NIR emission bands were observed *i.e.,* (Nd^{3+}: $^4F_{3/2} \rightarrow {}^4I_{9/2}$, Yb^{3+}: $^2F_{5/2} \rightarrow {}^2F_{7/2}$, Nd^{3+}: $^4F_{3/2} \rightarrow {}^4I_{11/2}$, and Nd^{3+}: $^4F_{3/2} \rightarrow {}^4I_{13/2}$) in co-doped glasses. NIR emission cross-sections [(σ_{emi}) stimulated, (σ^M_{emi}) from Mc-cumber theory] were calculated for $^2F_{5/2} \rightarrow {}^2F_{7/2}$ (~1030 nm) transition of Yb^{3+} ion. σ_{emi} was found to be highest (26.27×10^{-21} cm^2) for the Yb^{3+}: $^2F_{5/2} \rightarrow {}^2F_{7/2}$ transition in N2 glass. UC emission spectra recorded at 980 nm LD show bands centered at 500, 536, 595 & 610, and 664 nm, attributed to $^4G_{9/2} \rightarrow {}^4I_{9/2}$, $^4G_{7/2} \rightarrow {}^4I_{9/2}$& $^4G_{7/2} \rightarrow {}^4I_{11/2}$, $^4G_{5/2} \rightarrow {}^4I_{9/2}$, and $^4G_{9/2} \rightarrow {}^4I_{13/2}$ transitions, respectively. Decay profiles were analyzed for Yb^{3+}: $^2F_{5/2} \rightarrow {}^2F_{7/2}$ (~1030 nm) and Nd^{3+}: $^4F_{3/2} \rightarrow {}^4I_{11/2}$ (~1057 nm) transitions at 808 nm LD. Energy transfer (ET) process from Nd^{3+} to Yb^{3+} in present glasses were detailed.

1. Introduction

For the past several decades, trivalent rare-earth (RE^{3+})-doped or codoped optical materials like crystals, phosphors, and glasses have attracted a great deal of consideration from many materials science research groups for their different applications in areas such as solid-state lighting [1–3], lasers (NIR (near-infrared) and MIR (mid--infrared)) [4–8], fiber amplifiers [9–11], up-converters and down-converters for solar cells [12–15], temperature sensing devices [16,17], optoelectronics [18], radiation detection [19,20], atmospheric monitoring [21], biomedical imaging [22,23], etc.

Among different RE^{3+} ions, Yb^{3+} is unique owing to its having only two electronic energy levels ($^2F_{7/2}$ and $^2F_{5/2}$ only) in its structure with a wide energy gap (~10,256 cm^{-1}); it also shows both high σ_{abs} (absorption cross-section) and σ_{emi} in optical materials [24,25]. Usually, in glasses and crystals, Yb^{3+} ion exhibits a strong absorption band that normally peaks at ~980 nm wavelength; this material act as a sensitizer causing efficient ET (energy transfer) with minimal NR (non-radiative) decays when codoped with other RE^{3+} ions such as Er^{3+} [26,27], Tm^{3+} [28,29], Nd^{3+} [30–34], Pr^{3+} [35], and Ho^{3+} [36]. Next, Nd^{3+} ion as an activator gives different NIR emissions in crystals and glasses, with a band centered at about ~800–804 nm ($^4I_{9/2} \rightarrow {}^4F_{5/2}$) wavelength; this makes this material useful for absorbing maximum pump power and for obtaining low threshold, especially for NIR lasers; for example, bands centered at ~0.9 μm ($^4F_{3/2} \rightarrow {}^4I_{9/2}$), ~1.06 μm ($^4F_{3/2} \rightarrow {}^4I_{11/2}$), and ~1.33 μm ($^4F_{3/2} \rightarrow {}^4I_{13/2}$) in glasses are useful for laser and O-band amplification [37]. Due to its ladder-like arrangement of electronic energy levels, Nd^{3+} can show multiple absorption bands extending from UV (ultraviolet) to 820 nm Nd^{3+} can be easily pumped by commercially available low-cost 808 nm LD (laser diode) because it shows an intense

* Corresponding author.
** Corresponding author. Department of Physics, Chungnam National University, 99Daehak-ro, Yuseong-gu, Daejeon, 34134, South Korea.
E-mail addresses: drdevaprasadraju@gmail.com (B.D. Prasad Raju), mdkim@cnu.ac.kr (M.-D. Kim).

https://doi.org/10.1016/j.ceramint.2022.05.098
Received 12 March 2022; Received in revised form 28 April 2022; Accepted 8 May 2022
Available online 16 May 2022

and broad absorption ($^4I_{9/2} \rightarrow {}^4F_{5/2}$). Nd^{3+} ion can also yield MIR emissions at ~4.6 μm ($^4I_{9/2} \rightarrow {}^4I_{15/2}$) and ~5.8–4.7 μm ($^4I_{13/2} \rightarrow {}^4I_{11/2}$) wavelengths when utilized crystal or glass possesses relatively low phonon energy of ~450–500 cm^{-1} [38]. For example, both Yb^{3+} and Nd^{3+} ions are widely studied glasses and glass-ceramics to develop ~1 μm high-power ultra-short pulse lasers [31,34]. Also, in glasses and crystals, Nd^{3+} ion can produce UC (upconversion) emissions at ~ 0.59 μm ($^4G_{7/2} \rightarrow {}^4I_{11/2}$), ~0.658 μm ($^4G_{7/2} \rightarrow {}^4I_{13/2}$), and ~0.74 μm ($^4G_{7/2} \rightarrow {}^4I_{15/2}$) centered wavelengths under 808 nm LD excitation [39–41]. The first lasing process was reported by Snitzer [37] in Nd^{3+}-doped SiO_2-based glass.

Specifically, in comparison to crystals, RE^{3+}-doped glasses possess good photo-thermal features with minimal scattering centers, large absorption coefficients at pump wavelengths forming wide and intense optical bands, and high σ_{emi} (stimulated emission cross-sections) values, including high gain cross-sections for fiber laser and amplifier applications [6,42,43]. Compared to other oxide glasses, such as B_2O_3 [44], TeO_2 [45], GeO_2 [46], and P_2O_5-based [47] ones, SiO_2-based glasses show better chemical durability, and better mechanical and thermal stabilities for NIR lasers and optical amplifiers [48–52]. Owing to low-loss optical transmission window of SiO_2 fiber at 1200–1700 nm spectral range, this material is generally utilized in WDM (wavelength-division multiplexing) systems in telecommunications areas where different optical bands like O-(1260–1360 nm range), E–(1360–1460 nm span), S-(1460–1530 nm extent), C-(1530–1565 nm span), L-(1565–1625 nm range), and U-(1626–1675 nm span) are categorized in this NIR region [53]. In this regard, SiO_2-based EDFAs (Erbium-doped fiber amplifiers) and TDFAs (Thulium-doped fiber amplifiers) are developed and are in use for optical communication purposes [54,55].

In recent decades, ET materials made from Nd^{3+} to Yb^{3+} have been investigated in several different glass hosts, for instance in Refs. [30–34]. Parent et al. [30] investigated the microscopic parameters of Nd^{3+} and Yb^{3+} ions and found an excellent ET parameter, $C_{DA} = 16 \times 10^{-40}$ cm^6 S^{-1} in $LiLnP_4O_{12}$ meta-phosphate glasses. Sousa et al. [31] studied ET (Nd to Nd and Nd to Yb) processes in codoped fluoroindogallate glasses and found ET efficiency ~55% for 1Nd2Yb. Balda et al. [32] have examined $CaSiO_3$–$Ca_3(PO_4)_2$ eutectic glasses with Nd^{3+} and Yb^{3+} codoping and found an efficient ET ($Nd^{3+} \rightarrow Yb^{3+}$) could be obtained. Liegard et al. [33] described the Nd^{3+} to Yb^{3+} ET for the Yb^{3+} laser operation (980 nm) using an 808 nm excitation source for lead metaphosphate glasses and found less of an ET from Nd^{3+} to Yb^{3+} ions. Ding et al. [34] examined the optical and spectral characteristics of Nd^{3+} and Yb^{3+}-codoped tellurite glasses for NIR (1 μm) laser applications.

It is known that, when Al_2O_3 is included as an intermediate in glasses it can cause de-clustering of RE^{3+} ions, enhance refractive index, and improve thermal stability. Al_2O_3 can also improve radiative emissions by lowering phonon energy of glasses [55]. In SiO_2-based optical fibers, Al_2O_3 has been proven an effective additive for enhancing linear and non-linear refractive indices of glass and the spectroscopic features of doped RE^{3+} ions up to their CQ (concentration quenching) limit [55]. Na_2O addition can reduce melting points of glasses and also increase the glass viscosity [56]. The addition of alkali or alkaline earth fluorides (*e.g.,* CaF_2/SrF_2) to a glass composition can reduce OH^- groups and phonon energy [57,58].

Recently, NIR emissions, ET, and UC emissions of various RE^{3+}-doped oxyfluoride silicate glasses have been studied. For example, Duan et al. [29] reported the effect of CdF_2 on thermal and UC emissions (blue and red) in SiO_2–$AlO_{1.5}$–PbF_2–CdF_2–TmF_3–YbF_3 glasses. Zhu et al. [59] explored Dy- and Eu- doped SiO_2–Al_2O_3–ZnO–CaF_2–CaO glasses for LED (light emitting diode) applications by examing optical and visible fluorescence features at different excitation wavelengths.

Judd [60] and Ofelt [61] independently proposed a theory in 1962 referred to as J-O (Judd-Ofelt) theory for determining the line strengths or oscillation strengths of f–f optical transitions of RE ions in optical solids. Here, using J–O theory, three intensity parameters Ω_λ (λ = 2, 4, and 6) can be obtained and radiative factors such as A_R (radiative transition probability), β_R (branching ratio), and τ_R (radiative lifetime) for different excited levels of RE ions can also be predicted.

We recently reported Nd^{3+}–doped [62] glass compositions of SiO_2–Al_2O_3–Na_2O–SrF_2–CaF_2, in combination with Nd^{3+}/Yb^{3+} [63] and Yb^{3+}/Nd^{3+} [64]. In the current work, we explore optical, upconversion, and ~1.0 μm lasing features including fluorescence decay profiles for such SiO_2-based glasses with varied Nd^{3+} contents at fixed Yb^{3+} amount. From absorption spectra, J–O parameters (Ω_λ) (λ = 2, 4, and 6) are obtained and, using them, A_R, τ_R, and β_R for $^4F_{3/2}$ excited levels are computed.

2. Experimental

The SiO_2-based oxyfluoride glasses examined in this work have been prepared by melt-quench process in compositions of (44–*x*) SiO_2–5Al_2O_3–17Na_2O–18SrF_2–15CaF_2-1.0Yb_2O_3-*x*Nd_2O_3 (*x* = 0, 0.1, 0.5, 1.0, and 2.0 mol %). Attained glasses are coded as N0, N1, N2, N3, and N4, respectively, for convenience; details are provided in Table 1. Here, chemicals SiO_2 (99.8%), Al_2O_3 (99.99%), Na_2CO_3 (≥99.5%), SrF_2 (99.9%), CaF_2 (99.99%), Yb_2O_3 (99.9%), and Nd_2O_3 (99.9%), obtained from Sigma-Aldrich, were used for sample synthesis. Detailed glass synthesis procedures were provided in our earlier works [62,63]. ~30 g batches were mixed and ground for 30 min before collecting them in Al crucibles. Then, Al crucibles were closed with lid and placed in an electrical furnace in air atmosphere at 1400 °C for 1 h. The obtained liquids were transferred to a pre-heated brass sheet at 480 °C to obtain bulk glasses; these were annealed for 8 h at 480 °C to remove the

Table 1
Nominal chemical composition of the synthesized glasses (mol%).

Sample code	SiO_2	Al_2O_3	Na_2O	SrF_2	CaF_2	Yb_2O_3	Nd_2O_3
N0	44.0	5	17	18	15	1	0.0
N1	43.9	5	17	18	15	1	0.1
N2	43.5	5	17	18	15	1	0.5
N3	43.0	5	17	18	15	1	1.0
N4	42.0	5	17	18	15	1	2.0

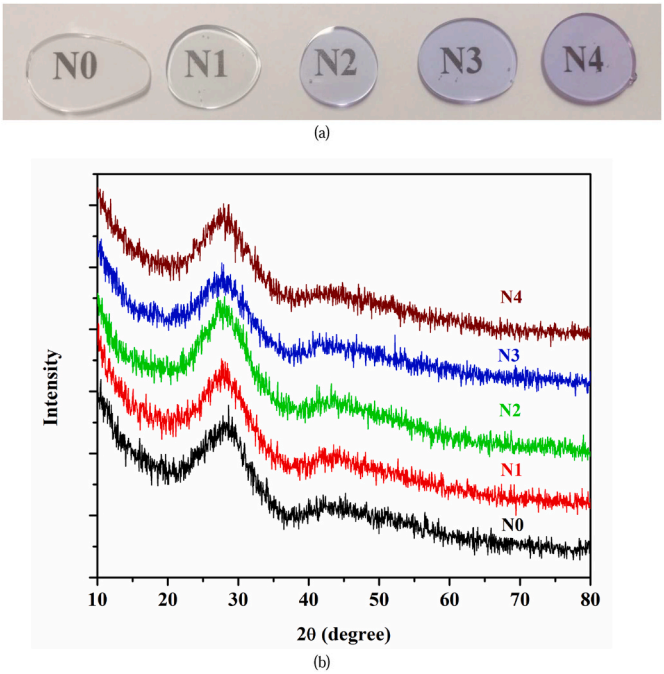

Fig. 1. (a) Photograph of all the studied glasses (b) X-ray diffraction (XRD) patterns of all the prepared glasses.

residual stresses. All acquired transparent glasses were polished using CeO_2 powder; polished sample images are presented in Fig. 1 (a).

Thickness (~1.5 mm) of all studied glasses was measured using digital Vernier calipers. Density (ρ) was determined with an error (±0.002 g/cm^3) by Archimedes' principle using distilled water as an immersion liquid. Refractive index (±0.001) was measured by Abbe refractometer at 589.3 nm wavelength. The sample structures were inspected by powder XRD (*X*-ray diffraction) (PANalytical) with monochromatic Cu–K_α radiation in the range of 10–80° (2θ) and with a resolution of 0.05°. FTIR spectra were recorded using a NICOLET 20 FTIR spectrometer with resolution of 1 cm^{-1}. Optical absorption spectra were recorded by a JASCO 770 spectrophotometer at 300–1100 nm wavelength span with a step size of 1 nm. NIR luminescence spectra were measured using an FLS980 fluorescence spectrometer under Xe lamp or 808 nm LD excitation with a resolution of 1 nm. A digital oscilloscope (Tektronix/DET10C) was used to acquire luminescence decay profiles with resolution of 0.001 ns. UC emission spectra were recorded using an FLS 980 spectrometer with 980 nm LD excitation and a resolution of 1 nm. To obtain comparable results for all studied glasses, during optical tests, we kept all sample positions, light incident angles, and thicknesses the same.

3. Results and discussion

3.1. Physical features

The different physical features considered for all synthesized glasses (N0–N4), and calculated following previous research [65,66] are exhibited in Table 2 (i). The measured refractive indices (n_d) increased in the order (1.5831–1.5851) for all synthesized glasses (N0–N1), evidently due to increasing Nd^{3+} ion in the glass compositions. The glass density (ρ) has usually been considered an important physical parameter. In Table 2 (i), it can be observed that 'ρ' values (3.0265–3.1282 g/cm^3) and average mol. weight (M) values (80.3372–85.8650 g/mol) increase with increases of dopant ion (Nd^{3+}) concentration (0–2.0 mol %) in all (N0–N4) glasses. In the present study, molar volume (V_m) gradually increased in range of (26.544–27.4487 cm^3/mol); this can be used to describe the glass network structure, because 'V_m' is directly proportional to 'ρ' and to the molecular weight of glasses. Other physical properties of RE (Yb^{3+}) ion concentration ($N_{Yb} = 2.269 \times 10^{20}$ ions/cm^3), interionic distance ($r_i = 16.3954$ Å), polaron radius ($r_p = 6.6073$ Å), and field strength ($F = 6.8717 \times 10^{14}$ cm^{-2}) were calculated using the relations [67] for N0 glass. For all the cations present in the glass composition, X_i (Pauling electronegativity), γ (optical basicity moderating parameters), and Λ (optical basicity) are given in Table 2 (ii). The 'γ' parameter is calculated for all oxide and fluoride species in the glass composition using a value of $\gamma = 1.36\,(X_i - 0.26)$ [67]. Optical basicity values of studied glasses were calculated using the relation from Ref. [68]; these values are presented in Table 2(i). The 'Λ' values gradually increase (0.5214 → 0.5328) with increasing Nd^{3+} ion concentration (0 → 2.0 mol %) in all (N0–N4) synthesized glasses; with the addition of Nd_2O_3 instead of SiO_2 increments of 'Λ' indicate the higher ability of oxide ions to donate electrons to surrounding cations.

3.2. Structural traits

3.2.1. XRD results

Fig. 1 (b) shows XRD patterns of all prepared glasses. XRD profiles did not shows any diffraction peaks in the range 10–80° for any of the studied (N0–N4) glasses, indicating their non-crystalline nature.

3.2.2. FTIR spectra

In the glass network, the alignment of structural units is determined using FTIR spectroscopy. The FTIR spectra of all prepared glass samples of SiO_2–Al_2O_3–Na_2O–SrF_2–CaF_2-Yb_2O_3–Nd_2O_3 studied at room temperature in the fingerprint region are (400–2000 cm^{-1}) shown in Fig. 2. Aluminosilicate and simple system silicate glasses have distinctive IR band covers (variably broken into separate bands) in the region of 1200–400 cm^{-1} [69,70]. It is predicted that the 655 cm^{-1} bands are derived from Si–O linkages, and a band centering at ~834 cm^{-1} is attributed to the stretching modes of Si–O–2NBO. A moderate infrared strength envelope extends from 800 to 650 cm^{-1}. Seifert et al. [71] reported that this envelope contains more than three perhaps component. McMillan et al. [72] proposed that the band at 834 cm^{-1} is primarily caused by motions of Si atoms against their oxygen tetrahedrons, as well as displacements of oxygen atoms associated with Si.

3.3. Absorption spectral studies

The absorption co-efficient spectra of N0–N4 glasses in the optical range from 300 to 1100 nm are presented in Fig. 3. The N0 spectrum has only one band *i.e.,* (Yb^{3+}: $^2F_{7/2} \rightarrow {}^2F_{5/2}$), but in the co-doped N0–N4 glasses the spectra consists of absorption bands of the Nd^{3+} ions *i.e.,* $^4D_{1/2}$, $^4D_{5/2}$, $^2P_{1/2}$, $^4G_{11/2}$ + (^2D, $^2P)_{3/2}$, $^4G_{9/2}$, $^4G_{7/2}$, $^4G_{5/2}$+$^2G_{7/2}$, $^2H_{11/2}$, $^4F_{9/2}$, $^4F_{7/2}$, $^2H_{9/2}$ and $^4F_{3/2}$, which are excited from the ground state ($^4I_{9/2}$) of Nd^{3+} ions it also contains the Yb^{3+}: $^2F_{7/2} \rightarrow {}^2F_{5/2}$ band together

Table 2
(i) Physical properties of silicate-based oxyfluoride glasses.

Physical parameter	N0	N1	N2	N3	N4
Refractive index, n_d (±0.001)	1.5831	1.5833	1.5841	1.5844	1.5851
Density, ρ, (g/cm^3) (±0.002)	3.0265	3.0270	3.0284	3.0793	3.1282
Avg. Mol. Weight (g/mol)	80.3372	80.6136	81.7191	83.1011	85.8650
Molar volume (cm^3/mol),	26.5446	26.6306	26.9843	26.987	27.4487
Oxygen packing density, OPD (mol/L)	46.3371	46.2250	45.7674	45.9480	45.5395
Molar refractivity, R_m (cm^3)	8.8726	8.9038	9.0321	9.0368	9.2004
Molar polarizability, α_m (×10^{-24} cm^3)	3.514	3.526	3.577	3.579	3.643
Glass optical basicity, Λ	0.5214	0.5220	0.5243	0.5272	0.5328

(ii) Glass elements optical basicity properties

Cation	Electronegitivity X_i	Basicity $\Lambda = \frac{0.75}{(X_i - 0.25)}$	Oxides			Fluorides		
			Basicity moderating parameter (γ)	Oxide	(Λ) $(\gamma)^{-1}$	Basicity moderating parameter (γ)	Fluoride	(Λ) $(\gamma)^{-1}$
Si^{4+}	1.9	0.4545	2.2304	SiO_2	0.4484			
Al^{3+}	1.61	0.5515	1.836	Al_2O_3	0.5447			
Na^{+}	0.93	1.1029	0.9112	Na_2O	1.0975			
Sr^{2+}	0.95	1.0714	0.9384	SrO	1.0656	2.1583	SrF_2	0.4633
Ca^{2+}	1	1	1.0064	CaO	0.9936	2.3147	CaF_2	0.4320
Yb^{3+}	1.1	0.8824	1.1424	Yb_2O_3	0.8754			
Nd^{3+}	1.14	0.8427	1.1968	Nd_2O_3	0.8356			

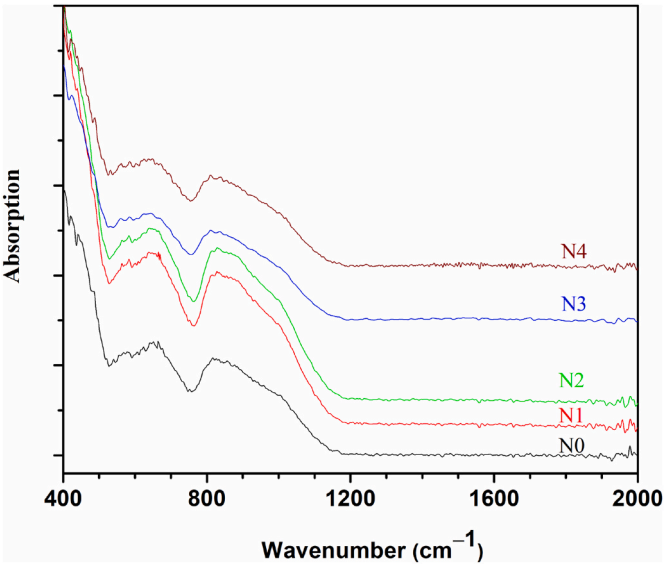

Fig. 2. IR spectra of all N0–N4 glasses.

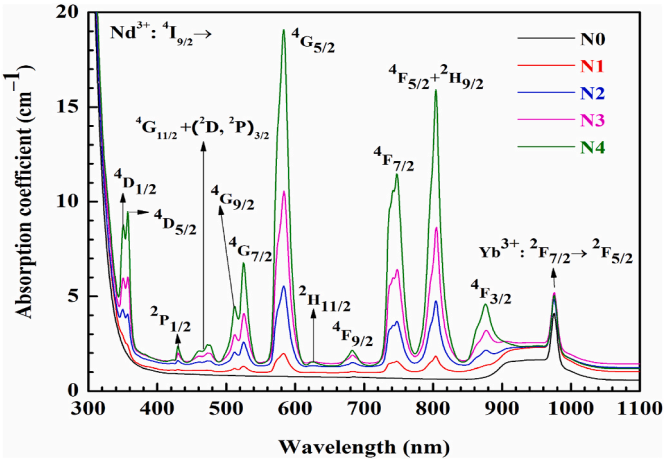

Fig. 3. Optical absorption spectra of all N0–N4 glasses.

with Nd^{3+}: $^4I_{9/2} \rightarrow {}^4F_{3/2}$. Consigned band positions and their relative transitions are well suited with the Nd^{3+} and Yb^{3+} transitions of other host glasses [46,47]. In-homogeneous broadening in the absorption transitions are due to the RE ions occupying sites that are not identical, i.e. crystal field strengths around individual RE ions are not homogeneous [42].

It is well-known that inorganic glasses, undoped or doped, with generally RE or transition metal (TM) ions, are non-direct or direct materials only owing to their amorphous structure; using the UV absorption spectra (Fig. S1 (a)) of our studied glasses, we evaluated the cutoff wavelengths ($\lambda_{cutt\text{-}off}$) and present them in Table 3. In Table 3, it can be see that $\lambda_{cutt\text{-}off}$ values move from 334 nm–341 nm for N0–N4 glasses, whereas for N1–N4 samples this range increases in the order N0 < N1 < N2 < N3 < N4 along with increasing Nd^{3+} ion concentration, indicating the effects of modifications on NBO creation in the present glass system.

The optical band gap (E_{opt}) values for all (N0–N4) glasses were determined in direct and indirect modes by following previous research [73]. All Tauc' plots are presented in Fig. S1 (supplementary file), *i.e.* (b) $h\nu$ vs. $(\alpha h\nu)^2$ *(direct) and (c)* $h\nu$ vs. $(\alpha h\nu)^{1/2}$ *(indirect)* were used to evaluate the optical bandgap (E_{opt}) of all N0–N4 glasses; values are presented in Table 3. The presence of Yb^{3+} ions and Nd^{3+} ions in the studied glasses (N0–N4), and E_{opt} values found in ranges of 3.957–3.931 eV and 3.644–3.594 eV for direct and indirect allowed transitions. Assumed E_{opt} values were changed only to induce possibly fewer alternations of NBOs (non–bridging oxygens) in the glass structure. The λ_g, $1/\lambda_g$, and $^{ASF}E_{opt}$ values were calculated via absorption spectrum fitting (ASF) using formulas of Souri et al. [74]; results are presented in Table 3. The plot of $(a\lambda^{-1})^{1/2}$ *vs.* λ^{-1} is shown in Fig. S1 (d); an estimated value of $^{ASF}E_g$ at $(a\lambda^{-1})^{1/2} = 0$ was obtained using linear region extrapolation. $^{ASF}E_{opt}$ values were found in the range of 3.656–3.610 eV, showing a similar trend to that of the direct and indirect values of all glasses for allowed and forbidden transitions.

The correlation among $h\nu$ and $ln(\alpha)$ was proposed by Urbach [75]; we calculated ΔE (Urbach energy) as follows:

$$\alpha(\nu) = \alpha_0 \exp\left(\frac{h\nu}{\Delta E}\right) \quad (1)$$

where α_0 = constant, h = Planck's constant. ΔE values are associated with variation of disordered materials like semiconductors, glasses, and insulators. From the relations of $h\nu$ and $ln(\alpha)$ shown in Fig. S1(e), ΔE values were calculated for all studied glasses (N0–N4) and found to be in a range of (0.2134–0.2419 eV); these are presented in Table 3. Overall, N0–N4 glasses retain their ΔE values (0.2134–0.2419 eV medium-range), signifying the presence of only minor defects in their structures; larger ΔE values typically denote high disorder and extensive distribution of localized EF (electric field forces) in the glass system [75].

In all our studied co-doped glass Yb^{3+}/Nd^{3+} samples, for J-O analysis we considered only Nd^{3+} ion related absorptions because the Yb^{3+} ion has only two energy levels, $^2F_{7/2}$ and $^2F_{5/2}$, and cannot provide transitions for J–O parameters calculations. In the literature, there are no reports on Yb^{3+} ion-doped glasses/crystals used for J–O analysis. J–O intensity factors have been calculated using details from a previous paper [62] for N1–N4 glasses; values are presented in Table 4. From these data, it is evident that samples N1 and N2 show a trend of $\Omega_2 < \Omega_4$

Table 4
JO intensity parameters ($\Omega_{2,\ 4,\ 6}$) of the N1-N4 glasses

Sample code	Ω_2	Ω_4	Ω_6	Trend
N1	4.728	7.414	7.041	$\Omega_2 < \Omega_4 < \Omega_6$
N2	4.995	8.393	7.375	$\Omega_2 < \Omega_4 < \Omega_6$
N3	5.575	6.999	7.370	$\Omega_2 < \Omega_6 > \Omega_4$
N4	5.957	6.109	6.524	$\Omega_2 < \Omega_6 > \Omega_4$

Table 3
Fundamental absorption edge (λ_{edge} ± 0.05 nm), direct optical band gap (E_{opt} ± 0.005 eV), indirect optical band gap (E_{opt} ± 0.005 eV), optical band gap evaluated through ASF method ($^{ASF}E_{opt}$ ± 0.005 eV), and Urbach energy (ΔE ± 0.002 eV) of all the N0–N4 glasses.

Sample Code	λ_{edge} (nm)	Direct optical band gap (eV) (n= 1/2)	Indirect optical band gap (eV) (n= 2)	$(1/\lambda_g)$ (nm^{-1})	λ_g (nm)	Optical band gap $^{ASF}E_{opt}$ (eV)	Urbach energy (eV)
N0	334	3.957	3.644	0.002948	339.213	3.656	0.2134
N1	336	3.950	3.633	0.002939	340.252	3.644	0.2216
N2	337	3.944	3.618	0.002932	341.064	3.636	0.2309
N3	339	3.937	3.607	0.002921	342.349	3.622	0.2338
N4	341	3.931	3.594	0.002911	343.525	3.610	0.2419

$< \Omega_6$ while trends of $\Omega_2 < \Omega_6 < \Omega_4$ are obtained for N3 and N4 glasses. Generally, factors Ω_2, Ω_4, and Ω_6 reveal bonding between ligand anions and RE ions; the bonded structures are adjacent to the RE ions sites. Here, the Ω_2 values increase from 4.728 to 5.957 $\times 10^{-20}$ cm^2 for all N1–N4 glasses, showing lower symmetry at less-abundant Nd^{3+} ion sites and higher covalence between ligand anions and Nd^{3+} ions. Both Ω_4 and Ω_6 values show the same trends for all studied glasses and reach their maximum values (8.393 and 7.375 $\times 10^{-20}$ cm^2) for N2 glass. To estimate the fluorescence factors of N1–N4 samples, radiative parameters such as A_R, β_R, and τ_R for optical transitions (Nd^{3+}: $^4F_{3/2} \rightarrow {}^4I_{9/2}$, $^4I_{11/2}$, $^4I_{13/2}$, and $^4I_{15/2}$) were computed using related J–O intensity factors; obtained outcomes are presented in Table 5 for N1–N4 glasses.

For all these calculations of radiative factors, conventional methods were applied as found in previous reports [61,62]. Higher values of A_R (~1978.2–2401.8 range) and β_R (~46–48%) for the $^4F_{3/2} \rightarrow {}^4I_{11/2}$ transition indicate its dominance for ~1.06 μm laser emission in all N1–N4 samples. Interestingly, there are increases of β_R (= 41–45%) for $^4F_{3/2} \rightarrow {}^4I_{9/2}$ (0.9 μm) laser transition for all N1 to N4 glasses. Further A_T values were in the range of 4076.8–5523.0 S^{-1} range for Nd^{3+}: $^4F_{3/2}$ excited level in N1–N4 glasses. The decrement of τ_R values in the range of 245–191 μs for N1–N4 glasses, due to the increment of Nd^{3+} concentration of 0.1–2.0 mol%.

3.4. NIR emission and Mc-Cumber theory

Fig. 4 shows the NIR emission spectra of all studied glasses (N0–N4) under excitation at 808 nm LD. Singly doped Yb^{3+} ions in (N0) glass did not show any emission peaks in the 830–1430 nm region. Though, when introducing the various concentrations (0.1–2.0 mol%) of Nd^{3+} ions in 1.0 mol% of Yb^{3+}-doped glasses (N1, N2, N3, and N4), intense emission bands were observed and are attributed to the Nd^{3+}: $^4F_{3/2} \rightarrow {}^4I_{9/2}$ (890 nm), $^4F_{3/2} \rightarrow {}^4I_{11/2}$ (1057 nm), $^4F_{3/2} \rightarrow {}^4I_{13/2}$ (1330 nm) and Yb^{3+}: $^2F_{5/2} \rightarrow {}^2F_{7/2}$ (1030 nm) transitions. The maximum emission intensity was observed at ~1030 nm in N2 glasses; it then decreased due to energy transfer from Yb^{3+} to Nd^{3+} ions.

Along with these values, NIR emission spectral analysis results of spectroscopic features such as σ_{abs} (absorption cross-section), effective bandwidth, σ_{emi} (emission cross-section) and pump saturation intensity were important in understanding enhancements of characteristics of Yb-doped laser materials. σ_{abs} is obtained from the absorption spectrum, using the following relation [76,77].

$$\sigma_{abs}(\lambda) = \frac{2.303 \times A}{Cl} \tag{2}$$

where A = absorbance, C = concentration of Yb^{3+} ions, and 'l' = thickness studied glasses.

A_{rad} (spontaneous emission probability), ($\Delta\lambda_{eff}$) fluorescence effective bandwidth, and σ_{emi} were calculated from emission spectra and absorption spectra of N0 glass materials using the following relations.

$$\Sigma_{abs} = \int \sigma_{abs}(\lambda) d\lambda = \int \frac{2.303 \times A}{Cl} d\lambda \tag{3}$$

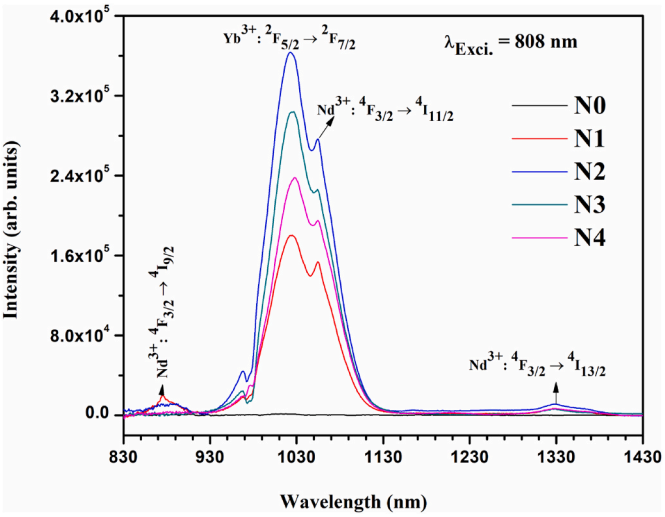

Fig. 4. NIR fluoroscence spectra of all N0–N4 glasses.

$$A_{rad} = \frac{1}{\tau_{rad}} = \frac{8\pi cn^2}{\lambda_P^4} \times \left(\frac{Z_u}{Z_l}\right) \times \Sigma_{abs} \tag{4}$$

where Σ_{abs} = integrated absorption cross-section, λ_p = peak wavelength, Z_u and Z_l denote as partition functions of upper ($^2F_{5/2}$) and lower ($^2F_{7/2}$) levels of Yb^{3+} ions, and σ_{emi} is the emission cross-section. A_{rad} (emission probability) is the $^2F_{5/2} \rightarrow {}^2F_{7/2}$ transition and 'n' is the RI (refractive index) of the present glasses.

σ_{emi} of the Yb^{3+}: $^2F_{5/2} \rightarrow {}^2F_{7/2}$ transition can be calculated with the Fuchtbauer–Ladenburg formula (F-L) [78] and the well-known Mc-Cumber theory [79].

$$\sigma_{emi}(\lambda) = \sigma_{abs}(\lambda) \frac{Z_l}{Z_u} \exp\left[\left(\frac{E_{Zl} - hc\lambda^{-1}}{k_B T}\right)\right] \tag{5}$$

E_{zl} (zero line energy) is representing the energy separation between $^2F_{5/2}$ and $^2F_{7/2}$ states of Yb^{3+} ion. 'h' = Planck's constant, k_B = Boltzmann's constant, and λ = 976 nm ($^2F_{7/2} \rightarrow {}^2F_{5/2}$ transition) of Yb^{3+} ions. σ_{abs} and σ_{emi} values were calculated for the Yb^{3+}: $^2F_{7/2} \rightarrow {}^2F_{5/2}$ (~976 nm) transition and are shown in Fig. 5 (N2 glass); remaining (N0, N1, N3, and N4 glasses) values are presented in Fig. S2 (a-d).

Cross-section values (σ_{abs} and σ_{emi}), Σ_{abs}, A_{rad}, and radiative lifetime (τ_R) values are calculated for all studied glasses and presented in Table 6 σ_{abs} and σ_{emi} values are found to be in the range 15.35–17.89 $\times 10^{-21}$ cm^2 and 23.45–26.37 $\times 10^{-21}$ cm^2 for all (N0–N4) glasses; these were compared with different compositions of Yb^{3+} ions doped materials with results shown in Table 6. For example, values include those of silicate (σ_{emi} = 7.7 $\times 10^{-21}$ cm^2) [80], 0.4MgF_2–0.4BaF_2–0.1$Al(PO_3)_3$–0.1Ba$(PO_3)_2$-1Yb_2O_3 (MBABP) (σ_{emi} = 8.7 $\times 10^{-21}$ cm^2) [81], 20Bi$(PO_3)_3$–10$Sr(PO_3)_2$–35BaF_2–35MgF_2–1Yb_2O_3 (BSBM) (σ_{emi} = 13.9 $\times 10^{-21}$ cm^2) [82], 20Na_2O–80B_2O_3–0.5Yb_2O_3 (σ_{emi} = 7.3 $\times 10^{-21}$ cm^2) [83], 30Na_2O–60P_2O_5–10Al_2O_3–0.5Yb_2O_3 (σ_{emi} = 5.7 $\times 10^{-21}$ cm^2) [83], 40K_2O–20Ta_2O_5–40Ga_2O_3–0.5Yb_2O_3 (σ_{emi} = 11.0 $\times 10^{-21}$ cm^2)

Table 5
Transitions, radiative transition probability (A_{rad}), branching ratio (β_R), for $^4F_{3/2} \rightarrow {}^4I_{9/2}$, $^4I_{11/2}$, $^4I_{13/2}$, and $^4I_{15/2}$ transition and radiative lifetime (τ_R) of Nd^{3+} ion in N1–N4 glasses.

Transitions	Sample code											
	N1			N2			N3			N4		
	A_{rad}	β_R	τ_{rad}	A_{rad}	β_R	τ_{rad}	A_{rad}	β_R	τ_{rad}	A_{rad}	β_R	τ_{rad}
$^4F_{3/2} \rightarrow {}^4I_{9/2}$	1693.4	0.415	245	2008.5	0.433	215	1941.4	0.417	214	2362.9	0.452	191
$^4F_{3/2} \rightarrow {}^4I_{11/2}$	1978.2	0.485		2196.7	0.473		2250.7	0.484		2401.8	0.460	
$^4F_{3/2} \rightarrow {}^4I_{13/2}$	385.8	0.095		415.2	0.089		437.5	0.094		436.7	0.084	
$^4F_{3/2} \rightarrow {}^4I_{15/2}$	19.08	0.005		20.53	0.004		21.63	0.005		21.60	0.004	
	A_T = 4076.8			**A_T = 4640.8**			**A_T = 4651.2**			**A_T = 5523.0**		

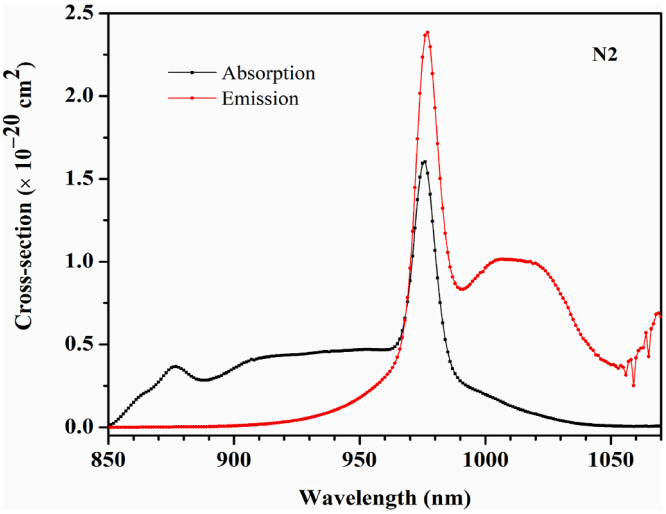

Fig. 5. Absorption and stimulated emission cross-section profiles of $^2F_{5/2} \rightarrow {}^2F_{7/2}$ transition in N2 glass.

[83], ZBLAN–1.0YbF$_3$ ($\sigma_{emi} = 5.1 \times 10^{-21}$ cm^2) [83], PbPhYb10 ($\sigma_{emi} = 6.5 \times 10^{-21}$ cm^2) [84], 60SiO$_2$–20Al$_2$O$_3$–20CaF$_2$–0.4YbF$_3$ ($\sigma_{emi} = 6.1 \times 10^{-21}$ cm^2) [85] glasses. Σ_{abs}, A_{rad}, and radiative lifetime (τ_R) values for all (N0–N4) studied glasses have the following ranges: Σ_{abs} = 5.882–9.609 p.m.^{2}, A_{rad} = 740.75–1213.17 s^{-1}, and τ_R = 1.350–0.8243 ms. Σ_{abs} and A_{rad} values increases with increasing Nd^{3+} concentration (0–2 mol%). Values of σ_{abs} ($^2F_{7/2} \rightarrow {}^2F_{5/2}$) = 17.89 × 10^{-21} cm^2 and σ_{emi} ($^2F_{5/2} \rightarrow {}^2F_{7/2}$) = 26.27 × 10^{-21} cm^2 are found to be highest for N2 glass; these results correlate with the emission profile. The very high value of σ_{emi} indicates that the present glasses might have potential as a medium to generate 1.0 μm laser applications.

Internal gain cross-section $G(\lambda)$ at wavelength λ can be estimated using the following formula:

$$G(\lambda,\gamma) = N[\gamma\sigma_{emi}(\lambda) - (1-\gamma)\sigma_{abs}(\lambda)]] \quad (6)$$

Here, N = concentration of Yb^{3+} and γ = fraction of electron population density for $^2F_{5/2}$ and $^2F_{7/2}$ levels of Yb^{3+} ions, where σ_{abs} and σ_{emi} are cross-sections obtained from Mc-Cumber theory. The wavelength dependence gain cross-section profiles for $^2F_{5/2} \rightarrow {}^2F_{7/2}$ transition were calculated for all glasses (N0–N4) and are shown in Fig. 6 (N2); the remaining values (N0, N1, N3, and N4 glasses) are presented in Fig. S3 (a—d). In all glass samples, the γ value varies from 0.0, 0.1, 0.3, 0.5, 0.7, to 1.0; when γ = 0.3, $G(\lambda)$ values progress in a positive manner. This is significant because a low pump threshold can be achieved. When γ is ≥ 0.3, $G(\lambda)$, the emission band moves to a longer wavelengths (from 975 nm to 1050 nm).

Studied glasses exhibit the largest gain at 976 nm; also, their broad emission (970–1130 nm) is favorable for the generation of tunable and ultrashort pulse lasers. Via analysis of gain cross-section, it can be stated that a wide tunable range of 975–1050 nm is expected in 1.0 mol% Yb^{3+}-ion doped oxyfluoride glasses. Spectroscopic and laser performance properties indicate that the studied glasses are encouraging materials for areas of optical amplification and lasers.

3.5. Energy transfer and spectroscopic properties under 808 nm LD excitation

The spectral overlap for the emission (Nd^{3+}: $^4F_{3/2} \rightarrow {}^4I_{9/2}$) and absorption (Yb^{3+}: $^2F_{7/2} \rightarrow {}^2F_{5/2}$) transitions in the range of 830–1040 nm are presented in Fig. 7 for N2 glass; remaining values are shown in Fig. S4 (a—d) for N0, N1, N3, and N4 glasses. These spectra represent the overlap stemming from the strong energy variation that exists within the excited state energy levels of Nd^{3+}: $^4F_{3/2}$ and Yb^{3+}: $^2F_{5/2}$, it should be noticed that the spectral overlap area increases with increasing concentration (0–2.0 mol%) of Nd^{3+} ions for all glasses.

The energy transfer parameter $C_{DA}^{Codoped}$ for co-doped (Yb^{3+}-Nd^{3+} ions) is determined using the overlapping of donor (Nd^{3+}: $^4F_{3/2} \rightarrow {}^4I_{9/2}$) emission and acceptor (Yb^{3+}: $^2F_{7/2} \rightarrow {}^2F_{5/2}$) absorption spectra, according to the following relations [86,87]:

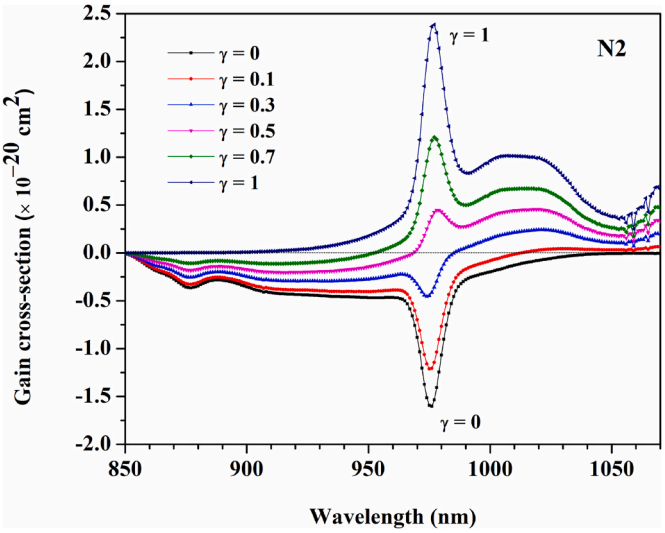

Fig. 6. Predicted theoretical gain spectra of $^2F_{5/2} \rightarrow {}^2F_{7/2}$ transition at γ = 0, 0.1, 0.3, 0.5, 0.7, and 1.0 of N2 glass.

Table 6
Absorption peak (λ_A), absorption cross-section (σ_{abs}), integrated absorption cross-section (Σ_{abs}), radiative transition probability (A_{rad}), emission cross-section (σ_{emi}) for $^2F_{7/2} \rightarrow {}^2F_{5/2}$ transition and radiative lifetime (τ_R) of Yb^{3+} in silicate based oxyfluride glasses.

Glass composition	λ_A (nm)	σ_{abs} (x 10^{-21} cm^2)	Σ_{abs} (× pm^2)	A_{rad} (s^{-1})	σ_{emi} (x 10^{-21} cm^2)	τ_R (ms)	References
N0	975	15.35	5.882	740.75	23.99	1.350	Present work
N1	975	16.03	6.934	874.34	23.84	1.144	Present work
N2	975	17.89	7.167	902.77	26.27	1.108	Present work
N3	975	16.50	8.051	1015.57	23.45	0.985	Present work
N4	975	16.74	9.609	1213.17	23.76	0.824	Present work
Silicate	975	24.0	–	–	7.7	–	[80]
0.4MgF$_2$–0.4BaF$_2$–0.1Al(PO$_3$)$_3$–0.1Ba(PO$_3$)$_2$-1Yb$_2$O$_3$ (MBABP)	976	16.4	–	1456	8.7	0.687	[81]
20Bi(PO$_3$)$_3$–10Sr(PO$_3$)$_2$–35BaF$_2$–35MgF$_2$–1Yb$_2$O$_3$ (BSBM)	977	17.7	–	1406	13.9	0.711	[82]
20Na$_2$O–80B$_2$O$_3$–0.5Yb$_2$O$_3$	974	–	4.78	1200	7.3	0.833	[83]
30Na$_2$O–60P$_2$O$_5$–10Al$_2$O$_3$–0.5Yb$_2$O$_3$	973	–	3.50	879	5.7	1.138	[83]
40K$_2$O–20Ta$_2$O$_5$–40Ga$_2$O$_3$–0.5Yb$_2$O$_3$	973	–	2.85	2420	11.0	0.413	[83]
ZBLAN–1.0YbF$_3$	973	–	2.80	834	5.1	1.199	[83]
PbPhYb10	976	9.6	–	499	6.5	2.004	[84]
60SiO$_2$–20Al$_2$O$_3$–20CaF$_2$–0.4YbF$_3$	975	11.7	–	506	6.1	1.196	[85]

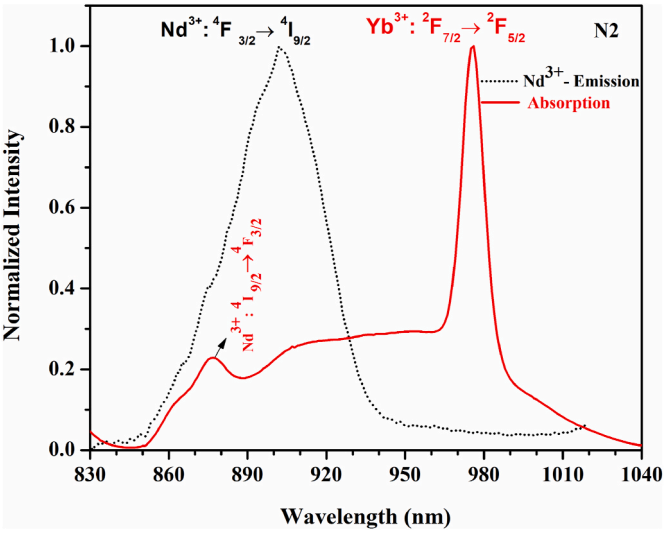

Fig. 7. Overlap spectra of Nd^{3+} ($^4F_{3/2} \rightarrow {}^4F_{9/2}$) emission and Yb^{3+} ($^2F_{7/2} \rightarrow {}^2F_{7/2}$) absorption of N2 glass.

$$C_{DA} = \frac{3c}{8\pi^4 n^2} \int \sigma^D_{em}(\lambda)\sigma^A_{abs}(\lambda)d\lambda \quad (7)$$

where, c = velocity of light in vacuum; n is the RI value of the present glasses, and "$\int \sigma^D_{em}(\lambda)\sigma^A_{abs}(\lambda)d\lambda$" represent the spectral overlap integral of the donor (Nd^{3+}: $^4F_{3/2} \rightarrow {}^4I_{9/2}$) emission and the acceptor (Yb^{3+}: $^2F_{7/2} \rightarrow {}^2F_{5/2}$) absorption cross-sections, respectively. ET parameter (C_{DA}^{YbNd}) value was calculated and found to be 14.176×10^{-38} cm^6 S^{-1} for N2 glasses. Furthermore, ET between Yb^{3+} and Nd^{3+} was investigated using photoluminescence spectra, decay analysis, partial energy level scheme of Yb^{3+} and Nd^{3+} ions, and ET parameters of (Nd^{3+}/Yb^{3+}) co-doped glasses. The obtained result show the influence of ET ($Nd^{3+} \rightarrow Yb^{3+}$) ions; further specific descriptions of radiative (emission) transitions and energy levels of Nd^{3+} and Yb^{3+} ions are presented in the energy level structure in Fig. 8.

When Nd–Yb co-doped glass samples were excited by the 808 nm LD, the ground state (Nd^{3+}: $^4I_{9/2}$) absorbed a photon and was excited to the $^4F_{5/2} + {}^2H_{9/2}$ state; it then relaxed to the $^4F_{3/2}$ level via NR relaxation process. Then, the ET from Nd^{3+}: $^4F_{3/2}$ to Yb^{3+}: $^2F_{5/2}$ ions was determined. Finally, emission at ~1030 nm occurred due to the Yb: $^2F_{5/2} \rightarrow {}^2F_{7/2}$ transition in the Yb^{3+}/Nd^{3+} co-doped glasses. The energy difference between the donor/sensitizer (Nd^{3+}) and acceptors/activator (Yb^{3+}) is not due to resonant energy; rather, it is due to host phonon-assisted energy only. The phonon energy (~1064 cm^{-1}) of the present silicate-based glasses was discussed in an earlier paper [63]. Our results confirm that ET from Nd^{3+} to Yb^{3+} can be observed in the studied (N0–N4) glasses and may be considered to be phonon-assisted energy transfer (PAET).

3.6. Upconversion studies

Fig. 9 presents up-conversion (UC) profiles (450–700 nm) of all studied (N0–N4) glasses, recorded under excitation of 980 nm LD. UC profile of N0 glass shows its strongest band at 500 nm of Yb^{3+} ions due to the cooperative luminescence [63]. Meanwhile, we observed four UC emission bands between the regions of 450–700 nm in co-doped (N1–N4) glasses. However, the N1–N4 glasses exhibit five UC emission bands, centered at 500 nm, 536 nm, 595 nm, 610 nm, and 664 nm, corresponding to the Nd^{3+}: $^4G_{9/2} \rightarrow {}^4I_{9/2}$, $^4G_{7/2} \rightarrow {}^4I_{9/2}$, $^4G_{7//2} \rightarrow {}^4I_{11/2}$, $^4G_{5/2} \rightarrow {}^4I_{9/2}$, and $^4G_{9/2} \rightarrow {}^4I_{13/2}$ transitions, respectively. UC emissions are confirmed to result from Nd^{3+} ions and indicate the potential of $Yb^{3+} \rightarrow Nd^{3+}$ ion energy transfer (ET), value λ_{exci} = 980 nm is in resonance with the Yb^{3+} transition $^2F_{7/2} \rightarrow {}^2F_{5/2}$. UC emission peak positions were found to be red shifted with increases Nd^{3+} ion concentration from 0 to 2 mol%.

The maximum UC emission intensity was observed in N1 glass; then, intensity decreased for the Nd^{3+}: $^4G_{9/2} \rightarrow {}^4I_{9/2}$, $^4G_{7/2} \rightarrow {}^4I_{9/2}$, $^4G_{5/2} \rightarrow {}^4I_{9/2}$ transitions with increasing Nd^{3+} ion concentration from 0.1 to 2.0 mol% in N1–N4 glasses. However, the UC emission intensity of the $^4G_{9/2} \rightarrow {}^4I_{13/2}$ (664 nm) transition rises with increases of Nd^{3+} ions in N1–N4 due to the lower number of non-radiative channels, as shown in the partial energy level diagram.

The energy level scheme of radiative transitions (emission lines) and non-radiative transitions of Nd^{3+} ions, and also their possible mechanisms, are clearly presented in Fig. 8. In this scheme, we distinguished two possible UC pathways. In the first case, the mechanism starts with resonant one-photon absorption by Yb^{3+}, followed by PAET to Nd^{3+}, which are originally in the ground state. But, in the second process, excited Nd^{3+} ions absorb photons at the $^4F_{3/2}$ state and advance to the $^4G_{11/2}$ level. They then decay NR (non-radiatively) to the $^4G_{9/2}$, which consequently decays radiatively to the ground state (at ~500 nm). Meanwhile, radiative transitions $^4G_{7/2} \rightarrow {}^4I_{9/2}$, $^4G_{7/2} \rightarrow {}^4I_{11/2}$, and $^4G_{5/2}$

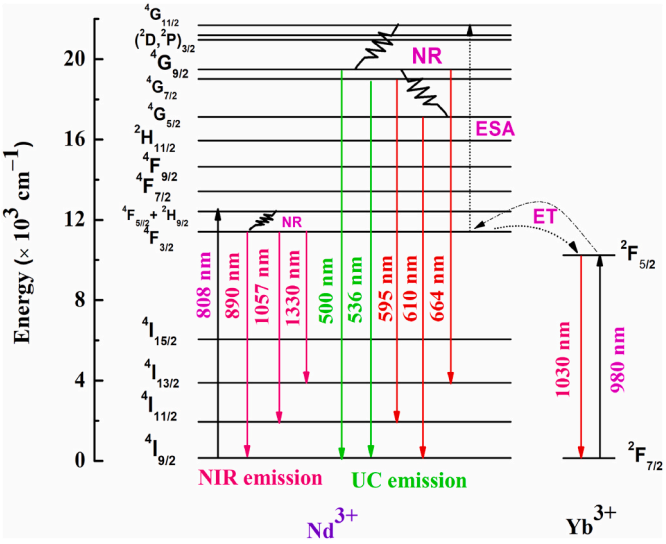

Fig. 8. Partial energy level diagram of all N0–N4 glasses under 808 and 980 nm excitations.

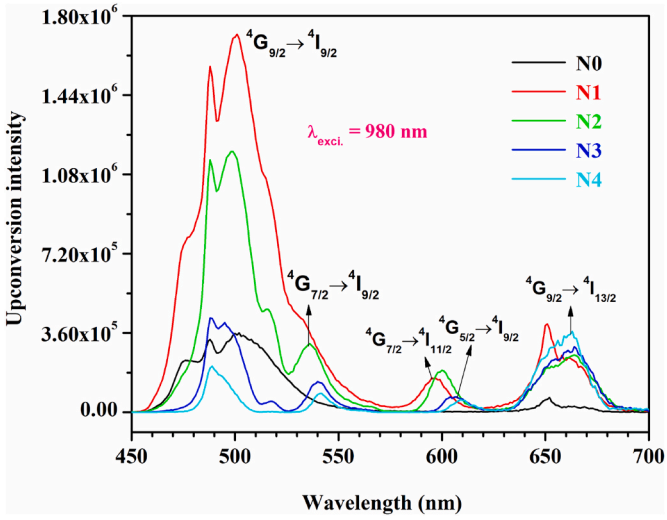

Fig. 9. Upconversion spectra of all N0–N4 glasses under 980 nm laser excitation.

→ $^4I_{9/2}$, were observed and found to be centered at ~536 nm, ~595, and ~610 nm, respectively. However, one more UC transition was observed from the $^4G_{9/2}$ → $^4I_{13/2}$ (~664 nm) transition of Nd^{3+} ions in codoped glasses.

3.7. Luminescence decay time analysis

The fluorescence decay profiles for the transition Yb^{3+}: $^2F_{5/2}$ → $^2F_{7/2}$ (~1030 nm) for N1, N2, N3, and N4 glasses are shown in Fig. 10. All decay curves showed non-exponential natures and lifetime values were calculated using the following expressions [62].

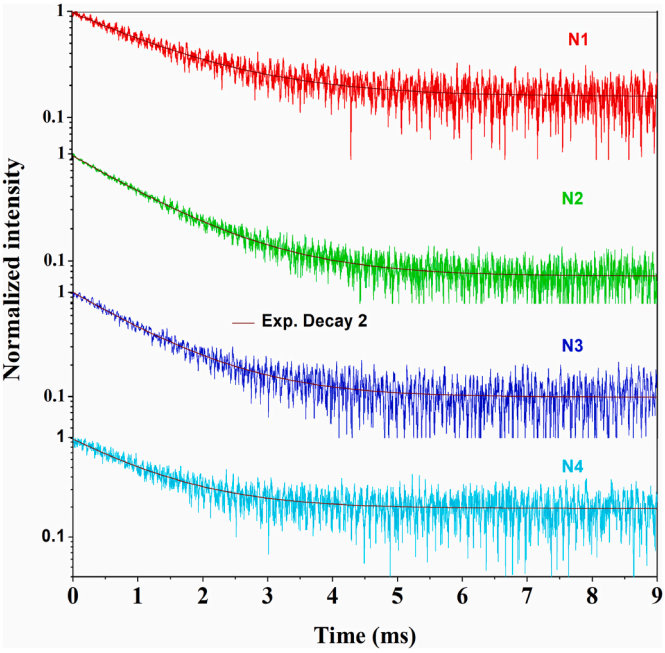

Fig. 10. Decay curves of $^2F_{5/2}$ level of all N1–N4 glasses under 808 nm excitation.

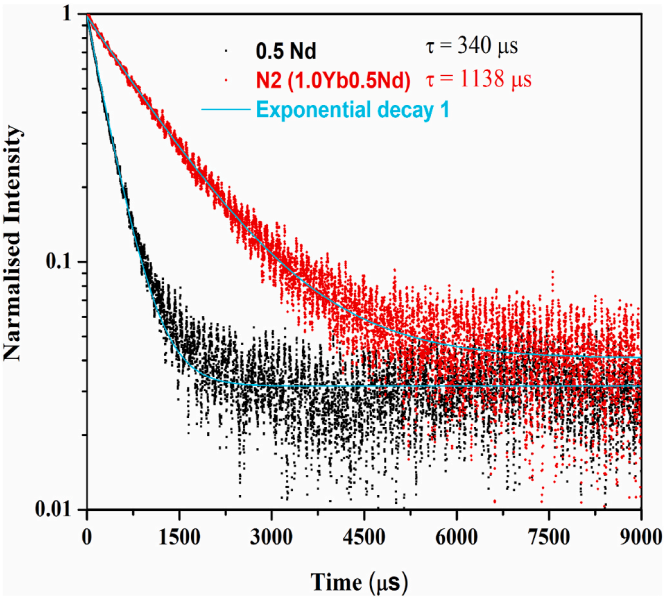

Fig. 11. Decay curves of $^4F_{3/2}$ level of 0.5Nd and N2 glasses under 808 nm excitation.

$$I(t) = A_1 \exp\left(\frac{-t}{\tau_1}\right) + A_2 \exp\left(\frac{-t}{\tau_2}\right) \quad (8)$$

where A_1 and A_2 are constants, and luminescence lifetimes τ_1 and τ_2 indicates two channels of fast and slow decay times, respectively. The value τ_{exp} (experimental lifetime) is calculated using the following relation:

$$\tau_{exp} = \frac{A_1\tau_1^2 + A_2\tau_2^2}{A_1\tau_1 + A_2\tau_2} \quad (9)$$

τ_{exp} values are 1.4047, 1.1793, 1.1197, and 1.1149 ms for N1, N2, N3, and N4 glasses respectively. τ_{exp} values decrease with increasing Nd^{3+} ion concentrations from 0.1 to 2.0 mol% in co-doped systems. τ_{exp} values of $^2F_{7/2}$ level are affected by the presence of Nd^{3+} ions and decrease from 1.4047 to 1.1149 ms, due to ET from Yb^{3+} to Nd^{3+} ions.

The decay profiles for the $^4F_{3/2}$ → $^4I_{11/2}$ (1057 nm) transition of Nd^{3+} ions in single (0.5) and co-doped (N2) glasses were recorded under λ_{exc} = 808 nm LD and are presented in Fig. 11. Decay profiles show non-exponential decay; calculated τ_{exp} value for 0.5Nd was 340 μs [62]; for N2 glass it was 1138 μs. τ_{exp} value of N2 glass was enhanced ~3 times compared to that of 0.5Nd glass, possibly because of the ET increase in Yb^{3+}→ Nd^{3+} ions in the studied glasses. Meanwhile, for the co-doped glasses, the ET process was mostly governed by electric dipole-dipole interaction, as revealed by Dexter theory. C_{DA} value was evaluated and found to be 14.176 × 10^{-38} cm^6 S^{-1} for N2 glass. Therefore, obtained results suggest that Yb^{3+} luminescence is sensitized by Nd^{3+} ions through the PAET process.

4. Conclusions

Yb^{3+}-singly and Yb^{3+}/Nd^{3+}-codoped silicate-based oxyfluoride glasses were examined for visible laser and NIR amplifier applications. The Ω_2 values increased from 4.728 to 5.957 × 10^{-20} cm^2 for all N1–N4 glasses; this indicates less symmetry in the presence of smaller amounts of Nd^{3+} ion and also the high covalency between ligand anions and Nd^{3+} ions. At λ_{exc} = 808 nm, four intense emission bands were centered at 890 nm, 1057 nm, 1330 nm (Nd^{3+}) and 1030 nm (Yb^{3+}). Yb^{3+} emission at ~1030 nm was achieved in co-doped samples owing to the ET from Nd^{3+} → Yb^{3+} ions. σ_{abs} ($^2F_{7/2}$ → $^2F_{5/2}$) was found to be higher value 17.89 × 10^{-21} cm^2 and σ_{emi} (for $^2F_{5/2}$ → $^2F_{7/2}$) was also evaluated and found to be 26.27 × 10^{-21} cm^2 in N2 glass. Intense up-converted emission peaks at 500 nm, 536 nm, 595 nm, 610 nm, and 664 nm were observed in N1–N4 glasses for visible lasers. We observed that UC emission red-shift follows increasing Nd^{3+} ion concentration, which shows the influence of the greater number of NR channels of the Nd^{3+} ions in the studied glasses. τ_{exp} values of the $^2F_{7/2}$ level are affected by the presence of Nd^{3+} ions and decrease from 1.4047 to 1.1149 ms due to ET from Yb^{3+} to Nd^{3+} ions. Meanwhile, τ_{exp} for the $^4F_{3/2}$ → $^4I_{11/2}$ transition (1138 μs) N2 glass was enhanced almost ~3 times compared to that of 0.5Nd glass (340 μs). The ET parameter (C_{DA}) is calculated and found to be 14.176 × 10^{-38} cm^6 S^{-1} for N2 glass. These results indicate that RE concentrations (1 Yb^{3+}/0.5 Nd^{3+}) should be optimized to understand the possibility and potential of Nd^{3+}→Yb^{3+} and Yb^{3+}→Nd^{3+} ET in optical materials. The high value of σ_{emi} indicates that N2 glass can be a potential medium to generate ~1.0 μm laser applications.

Declaration of competing interest

The authors declare that they have no known competing financial interests or personal relationships that could have appeared to influence the work reported in this paper.

Acknowledgements

This work was supported by the Basic Science Research Program

through the National Research Foundation of Korea (NRF) funded by the Ministry of Science and ICT (Grant No. 2020R1A2C2013385), the Ministry of Education (NRF-2020R1A6A1A03047771), and also supported from the Korea Institute for Advancement of Technology (KIAT) grant funded by the Korean Government (MOTIE) (P0008458, HRD Program for Industrial Innovation).

Appendix A. Supplementary data

Supplementary data to this article can be found online at https://doi.org/10.1016/j.ceramint.2022.05.098.

References

[1] T. Justel, H. Nikol, C. Ronda, New developments in the field of luminescent materials for lighting and displays, Angew. Chem. Int. Ed. 34 (1998) 3084–3103, https://doi.org/10.1002/(SICI)1521-3773(19981204)37:22<3084::AID-ANIE3084>3.0.CO;2-W.

[2] C. Feldmann, T. Justel, C.R. Ronda, P.J. Schmidt, Inorganic luminescence materials: 100 years of research and applications, Adv. Funct. Mater. 13 (2003) 511–516, https://doi.org/10.1002/adfm.200301005.

[3] N.C. George, K.A. Denault, R. Seshadri, Phosphors for solid state white lighting, Annu. Rev. Mater. Res. 43 (2013) 481–501. 10.1146/annurev-matsci-073012-125702.

[4] P.D. Dragic, M. Cavillon, J. Ballato, Materials for optical fiber lasers: a review, Appl. Phys. Rev. 5 (2018), 041301, https://doi.org/10.1063/1.5048410.

[5] T.S. McComb, R.A. Sims, Christina C.C. Willis, P. Kadwani, V. Sudesh, L. Shah, M. Richardson, High-power widely tunable thulium fiber lasers, Appl. Opt. 49 (2010) 6236–6242, https://doi.org/10.1364/AO.49.006236.

[6] A. Jha, B. Richards, G. Jose, T. Teddy-Fernandez, P. Joshi, X. Jiang, J. Lousteau, Rare-earth ion doped TeO_2 and GeO_2 glasses as laser materials, Prog. Mater. Sci. 57 (2012) 1429–1491. 10.1016/j.pmatsci.2012.04.003.

[7] J.R. Armitage, Introduction to glass fibre lasers and amplifiers, in: P.W. France (Ed.), Optical Fibre Lasers and Amplifiers, Blackie and Sons, Ltd., London, 2000, pp. 14–38.

[8] S.D. Jackson, Towards high-power mid-infrared emission from a fibre laser, Nat. Photonics 6 (2012) 423–431. https://www.nature.com/articles/nphoton.2012.149.pdf.

[9] M.J.F. Digonnet, Rare Earth Doped Fiber Lasers and Amplifiers, second ed., Marcel Dekker Inc., New York, NY, 1993.

[10] W.J. Miniscalco, Erbium-doped glasses for Fiber amplifiers at 1500 nm, J. Lightwave Technol. 9 (1991) 234–250, https://doi.org/10.1109/50.65882.

[11] S. Tanabe, Rare-earth-doped glasses for fiber amplifiers in broadband telecommunication, Compt. Rendus Chem. 5 (2002) 815–824, https://doi.org/10.1016/S1631-0748(02)01449-2.

[12] F. Auzel, Upconversion and anti-Stokes processes with f and d ions in solids, Chem. Rev. 104 (2004) 139–173, https://doi.org/10.1021/cr020357g.

[13] J.D. Wild, A. Meijerink, J.K. Rath, W.G.J.H.M. van Sark, R.E.I. Schropp, Upconverter solar cells: materials and applications Energy, Environ. Sci. 4 (2011) 4835, https://doi.org/10.1039/c1ee01659h.

[14] M.V. Bryan M. van der Ende, Aarts Linda, A. Meijerink, Lanthanide ions as spectral converters for solar cells, Phys. Chem. Chem. Phys. 11 (2009) 11081–11095, https://doi.org/10.1039/b913877c.

[15] R.T. Wegh, H. Donker, K.D. Oskam, A. Meijerink, Visible quantum cutting in $LiGdF_4$:Eu^{3+} through downconversion, Science 283 (1999) 663–666, https://doi.org/10.1126/science.283.5402.663.

[16] F. Vetrone, R. Naccache, A. Zamarron, A. Juarranz de la Fuente, F. Sanz-Rodriguez, L. Martinez Maestro, E. Martin Rodriguez, D. Jaque, J. Garcia Sole, A. John Capobianco, Temperature sensing using fluorescent nanothermometers, ACS Nano 4 (2010) 3254–3258, https://doi.org/10.1021/nn100244a.

[17] D. Wawrzynczyk, A. Bednarkiewicz, M. Nyk, W. Strek, M. Samo, Neodymium (III) doped fluoride nanoparticles as non-contact optical temperature sensors, Nanoscale 4 (2012) 6959–6961, https://doi.org/10.1039/c2nr32203j.

[18] A.J. Kenyon, Recent developments in rare-earth doped materials for optoelectronics, Prog. Quant. Electron. 26 (2002) 225–284, https://doi.org/10.1016/S0079-6727(02)00014-9.

[19] F. Caputo, M. De Nicola, A. Sienkiewicz, A. Giovanetti, I. Bejarano, S. Licoccia, E. Traversab, L. Ghibelli, Cerium oxide nanoparticles, combining antioxidant and UV shielding properties, prevent UV-induced cell damage and mutagenesis, Nanoscale 7 (2015) 15643, https://doi.org/10.1039/c5nr03767k.

[20] T. Kuro, G. Okada, N. Kawaguchi, Y. Fujimoto, H. Masai, T. Yanagida, Scintillation properties of rare-earth doped NaPO3-Al(PO3)3 glasses, Opt. Mater. 62 (2016) 561–568, https://doi.org/10.1016/j.optmat.2016.11.018.

[21] M. Fibrich, J. Sulc, R. Kral, V. Jary, M. Nemec, H. Jelinkova, A. Bystricky, P. Zemenova, M. Nikl, Luminescence study of rare-earth (RE)-doped low-energy phonon $RbPb_2Cl_5$ crystals for mid-infrared (IR) lasers emitting above 4.5 μm wavelength, Laser Phys. 29 (2019), 075801, https://doi.org/10.1088/1555-6611/ab1481.

[22] H.N. Luitel, R. Chand, T. Torikai, M. Yada, T. Watari, Highly efficient NIR–NIR upconversion in potassium substituted $CaMoO_4$:Tm^{3+}, Yb^{3+} phosphor for potential biomedical applications, RSC Adv. 5 (2015) 17034, https://doi.org/10.1039/C4RA12436G.

[23] D.S.B. Carlos, S. Balabhadra, L.D. Carlo, Lanthanide-based thermometers: at the cutting-edge of luminescence thermometry, Adv. Opt. Mater. 7 (2019), 1801239, https://doi.org/10.1002/adom.201801239.

[24] G. Boulon, Why so deep research on Yb^{3+}-doped optical inorganic materials, J. Alloys Compd. 451 (2008) 1–11, https://doi.org/10.1016/j.jallcom.2007.04.148.

[25] L.R.P. Kassab, Sonia H. Tatumi, A.S. Morais, L.C. Courrol, N.U. Wetter, V.L. R. Salvador, Spectroscopic properties of lead fluoroborate glasses doped with ytterbium, Opt Express 8 (2001) 585–589, https://doi.org/10.1364/OE.8.000585.

[26] E. Kolobkova, A. Alkhlef, A. Yasukevich, A. Babkina, Spectroscopic and lasing properties of Er^{3+}/Yb^{3+}-doped fluorophosphate glass with small additives of phosphates, Opt. Mater. Express 9 (2019) 3666–3679, https://doi.org/10.1364/OME.9.003666.

[27] J.F. Philipps, T. Töpfer, H. Ebendorff-Heidepriem, D. Ehrt, R. Sauerbrey, Spectroscopic and lasing properties of Er^{3+}:Yb^{3+}-doped fluoride phosphate glasses, Appl. Phys. B 72 (2001) 399–405, https://doi.org/10.1007/s003400100515.

[28] F.C. Guinhos, P.C. Nobrega, P.A. Santa-Cruz, Compositional dependence of up-conversion process in Tm–Yb codoped oxyfluoride glasses and glass-ceramics, J. Alloys Compd. 323–324 (2001) 358–361, https://doi.org/10.1016/S0925-8388(01)01036-2.

[29] Z. Duan, J. Zhang, D. He, H. Sun, L. Hu, Effect of CdF_2 addition on thermal stability and upconversion luminescence properties in Tm^{3+}–Yb^{3+} codoped oxyfluoride silicate glasses, Mater. Chem. Phys. 100 (2006) 400–403, https://doi.org/10.1016/j.matchemphys.2006.01.022.

[30] C. Parent, C. Lurin, G. Le Flem, P. Hagenmuller, Nd^{3+} → Yb^{3+} energy transfer in glasses with composition close to $LiLnP_4O_{12}$ metaphosphate (Ln = La, Nd, Yb), J. Lumin. 36 (1986) 49–55, https://doi.org/10.1016/0022-2313(86)90030-X.

[31] D.F. Sousa, F. Batalioto, M.J.V. Bell, S.L. Oliveira, L.A.O. Nunes, Spectroscopy of Nd^{3+} and Yb^{3+} codoped fluoroindogallate glasses, J. Appl. Phys. 90 (2001) 3308–3313, https://doi.org/10.1063/1.1397289.

[32] R. Balda, J.I. Pena, M.A. Arriandiaga, J. Fernandez, Efficient Nd^{3+}→Yb^{3+} energy transfer in $0.8CaSiO_3$-$0.2Ca_3(PO_4)_2$ eutectic glass, Opt Express 18 (2010) 13842–13850, https://doi.org/10.1364/oe.18.013842.

[33] F. Liegard, J.L. Doualan, R. Moncorge, M. Bettinelli, Nd^{3+} → Yb^{3+} energy transfer in a codoped metaphosphate glass as a model for Yb^{3+} laser operation around 980 nm, Appl. Phys. B 80 (2005) 985–991, https://doi.org/10.1007/s00340-005-1829-y.

[34] N. Ding, J. Diao, D. Zhang, T. Zheng, Jingwen Lv, Spectroscopic properties of Yb^{3+} and Nd^{3+} co-doped tellurite glass for 1.0 μm laser application, Ceram. Int. 46 (2020) 25633–25637, https://doi.org/10.1016/j.ceramint.2020.07.038.

[35] G. Gao, L. Wondraczek, Near-infrared downconversion in Pr^{3+}/Yb^{3+} co-doped boro-aluminosilicate glasses and $LaBO_3$ glass ceramics, Opt. Mater. Express 3 (2013) 633–644, https://doi.org/10.1364/OME.3.000633.

[36] W. Cao, F. Huang, R. Ye, M. Cai, R. Lei, J. Zhang, S. Xu, X. Zhang, Structural and fluorescence properties of Ho3+/Yb3+ doped germanosilicate glasses tailored by Lu2O3, J. Alloys Compd. 746 (2018) 540–548, https://doi.org/10.1016/j.jallcom.2018.02.325.

[37] E. Snitzer, Optical maser action of Nd^{+3} in a barium crown glass, Phys. Rev. Lett. 7 (1961) 444–446, https://doi.org/10.1103/PhysRevLett.7.444.

[38] R. Reisfeld, C.K. Jorgensen, Lasers and Excited States of Rare Earths, Springer-Verlag, Berlin, 1977, https://doi.org/10.1007/978-3-642-66696-4.

[39] T.T. Basiev T.T. Yu. V. Orlovskii, I. N. Vorobev, L. N. Dmitruk, T. D. Efimenko, V. A. Konyushkin, V. V. Osiko, Relaxation of mid-IR transitions of Nd^{3+} in laser crystals with "short" phonon spectra. In: Krupa JC., Kulagin N.A. (eds) Physics of Laser Crystals. NATO Science Series (Series II: Mathematics, Physics and Chemistry), vol. 126. Springer, Dordrecht. https://doi.org/10.1007/978-94-010-0031-4_4.

[40] D.S. da Silva, T.A.A. de Assumpçao, L.R.P. Kassab, C.B. de Araujo, Frequency upconversion in Nd3+ doped PbO–GeO2 glasses containing silver nanoparticles, J. Alloys Compd. 586 (2014) S516–S519, https://doi.org/10.1016/j.jallcom.2012.12.070.

[41] J. Suresh Kumar, K. Pavani, S.R. Gavinho, M. Seshadri, V. Anjos, M.J.V. Bell, F. N. Freire, M.A. Valente, M.J. Soares, M.P.F. Graça, Temperature dependent upconversion and spectroscopic properties of Nd3+ doped barium bismuth tellurite glasses, J. Non-Cryst. Solids 498 (2018) 89–94, https://doi.org/10.1016/j.jnoncrysol.2018.05.031.

[42] R.S. Quimby, Output saturation in a 980-nm pumped erbium-doped fiber amplifier, 2546, Appl. Opt. 30 (1991) 2546–2552, https://doi.org/10.1364/AO.30.002546.

[43] K. Li, S. Fan, L. Zhang, Q. Zhang, J. Zhang, L. Hu, Spectroscopic properties of the 1.8 μm emission of Tm3+/Yb3+ codoped TeO2–ZnO–Bi2O3 glasses with efficient energy transfer, J. Non-cryst. Solid. 357 (2011) 2417–2420, https://doi.org/10.1016/j.jnoncrysol.2010.12.022.

[44] Y.D. Yiannopoulos, G.D. Chryssikos, E.I. Kamitsos, Structure and properties of alkaline earth borate glasses, Phys. Chem. Glasses 42 (2001) 164–172. https://www.ingentaconnect.com/contentone/sgt/pcg/2001/00000042/00000003/4203164.

[45] J.J. Leal, E. Rodriguez, C.G. Nava-Dino, M.C. Maldonado-Orozco, F. Gaxiola, R. Narro-Garcia, Effect of Ho3+ concentration on the luminescent and thermal stability of tellurite glasses, Mater. Res. Bull. 144 (2021), 111483, https://doi.org/10.1016/j.materresbull.2021.111483.

[46] A. Herrera, F. Londoño, N.M. Balzaretti, Structural and optical properties of Nd3+ doped GeO2-PbO glass modified by TiO2 for applications in laser and fiber amplifier, Opt. Mater. 113 (2021), 110884, https://doi.org/10.1016/j.optmat.2021.110884.

[47] J.H. Campbell, T.I. Suratwala, Nd-doped phosphate glasses for high-energy/high-peak-power lasers, J. Non-Cryst. Solids 263 (2000) 318–341, https://doi.org/10.1016/S0022-3093(99)00645-6, 264.

[48] H. Zeng, J. Qiu, S. Yuan, Y. Yang, G. Chen, Precipitation of metallic nanoparticles inside silicate glasses by femtosecond laser pulses, Ceram. Int. 34 (2008) 605–608, https://doi.org/10.1016/j.ceramint.2006.12.011.

[49] Z. Wang, F. Huang, B. Li, Y. Li, Y. Tian, S. Xu, Enhanced luminescence properties of Ho/Yb ions regulated by the nanocrystalline environment and phonon energy in silicate glasses, J. Lumin. 219 (2020), 116949, https://doi.org/10.1016/j.jlumin.2019.116949.

[50] S.D. Jackson, The spectroscopic and energy transfer characteristics of the rare earth ions used for silicate glass fibre lasers operating in the shortwave infrared, Laser Photon. Rev. 3 (2009) 466–482, https://doi.org/10.1002/lpor.200810058.

[51] M. Li, Y.Y. Guo, G.X. Bai, Y. Tian, L.L. Hu, J.J. Zhang, ~2 μm luminescence and energy transfer characteristics in Tm^{3+}/Ho^{3+}co-doped silicate glass, J. Quant. Spectrosc. Radiat. Transf. 127 (2013) 70–77, https://doi.org/10.1016/j.jqsrt.2013.04.025.

[52] M. Wang, Q. Zheng, A. Chen, Y. Li, X. Zhang, D. Zhang, S. Jin, D. Xiong, W. Deng, Crystallization, thermal expansion and hardness of Y2O3–Al2O3–SiO2 glasses, Ceram. Int. 47 (2021) 25059–25066, https://doi.org/10.1016/j.ceramint.2021.05.236.

[53] S.V. Firstov, S.V. Alyshev, K.E. Riumkin, V.F. Khopin, A.N. Guryanov, M. A. Melkumov, E.M. Dianov, A 23-dB bismuth-doped optical fiber amplifier for a 1700-nm band, Sci. Rep. 6 (2016) 28939, https://doi.org/10.1038/srep28939.

[54] S.D. Jackson, Cross relaxation and energy transfer upconversion processes relevant to the functioning of 2 μm Tm^{3+}-doped silica fibre lasers, Opt Commun. 230 (2004) 197–203, https://doi.org/10.1016/j.optcom.2003.11.045.

[55] X. Song, D. Zhou, P. Xu, K. Han, C. Song, ~2 μm fluorescence and energy transfer characteristics in a highly Tm^{3+}-doped bismuthate glass based on Al_2O_3 adjustment, Opt. Mater. Express 11 (2021) 3755–3767, https://doi.org/10.1364/OME.438033.

[56] Q. Zhao, M. Guerette, G. Scannell, L. Huang, In-situ high temperature Raman and Brillouin light scattering studies of sodium silicate glasses, J. Non-Cryst. Solids 358 (2012) 3418–3426, https://doi.org/10.1016/j.jnoncrysol.2012.04.034.

[57] C. Bocker, J. Wiemert, C. Rüssel, The formation of strontium fluoride nano crystals from a phase separated silicate glass, J. Eur. Ceram. Soc. 33 (2013) 1737–1745, https://doi.org/10.1016/j.jeurceramsoc.2013.02.008.

[58] M. Stoica, A. Herrmann, J. Hein, C. Russel, UV–vis spectroscopic studies of CaF2 photo-thermo-refractive glass, Opt. Mater. 62 (2016) 424–432, https://doi.org/10.1016/j.optmat.2016.10.031.

[59] C. Zhu, X. Zhang, H. Ma, C. Timlin, Sb-, Dy-, and Eu-doped oxyfluoride silicate glasses for light emitting diodes, J. Alloys Compd. 647 (2015) 880–885, https://doi.org/10.1016/j.jallcom.2015.05.186.

[60] B.R. Judd, Optical absorption intensities of rare-earth ions, Phys. Rev. 127 (1962) 750–761, https://doi.org/10.1103/PhysRev.127.750.

[61] G.S. Ofelt, Intensities of crystal spectra of rare-earth ions, J. Chem. Phys. 37 (1962) 511–520, https://doi.org/10.1063/1.1701366.

[62] G. Devarajulu, P.S. Prasad, N.J. Sushma, C.M. Reddy, S. Chourasia, B.D.P. Raju, Effect of neodymium ions on upconversion fluorescence studies of oxyfluorosilicate glasses for optoelectronic devices, Ceram. Int. 43 (2017) 16076–16083, https://doi.org/10.1016/j.ceramint.2017.08.123.

[63] G. Umamaheswar, G. Devarajulu, M. Rajesh, B. Ramesh, N.J. Sushma, V. Ramasamy, B.D.P. Raju, Study of optical properties and up-conversion mechanism in Nd^{3+}/Yb^{3+} ions co-doped SiO_2–Al_2O_3–Na_2CO_3–SrF_2–CaF_2 glasses for green light emitting display device applications, Optik 171 (2018) 918–924, https://doi.org/10.1016/j.ijleo.2018.06.119.

[64] G. Umamaheswar, G. Devarajulu, V. Ramaswamy, B.D.P. Raju, Spectroscopic properties of Yb^{3+}/Nd^{3+} co-doped ions in SiO_2–Al_2O_3–Na_2CO_3–SrF_2–CaF_2 oxyfluoride glasses for photonic applications, Photon. Lett. Pol. 10 (2018) 29–31.

[65] G.V. Prakash, R. Jagannathan, D.N. Rao, Physical and optical properties of NASICON-type phosphate glasses, Mater. Lett. 57 (2002) 134–140, https://doi.org/10.1016/S0167-577X(02)00719-X.

[66] M.I. Sayyed, G. Lakshminarayana, M. Moghaddasi, I.V. Kityk, M.A. Mahdi, Physical Properties, Optical band gaps and radiation shielding parameters exploration for Dy^{3+}-doped alkali/mixed alkali multicomponent borate glasses, Glass Phys. Chem. 44 (2018) 279–291, https://doi.org/10.1134/S1087659618040119.

[67] A. Duffy, A common optical basicity scale for oxide and fluoride glasses, J. Non-Cryst. Solids 109 (1989) 35–39, https://doi.org/10.1016/0022-3093(89)90438-9.

[68] Z. Hussain, Optical band gap, oxidation polarizability, optical basicity and electronegativity measurements of silicate glasses using ellipsometer and Abbe refractometer, New J. Glass Ceram. 11 (2021) 1–33, https://doi.org/10.4236/njgc.2021.111001.

[69] W.R. Taylor, Application of infrared spectroscopy to studies of silicate glass structure: examples from the melilite glasses and the systems Na_2O-SiO_2 and Na_2O-Al_2O_3-SiO_2, Proc. Indian Acad. Sci. 99 (1990) 99–117.

[70] M. Sitarz, The structure of simple silicate glasses in the light of Middle Infrared spectroscopy studies, J. Non-Cryst. Solids 357 (2011) 1603–1608, https://doi.org/10.1016/j.jnoncrysol.2011.01.007.

[71] F. Seifert, B.O. Mysen, D. Virgo, Three-dimensional network structure of quenched melts (glass) in the systems SiO_2-$NaAlO_2$, SiO_2-$CaAl_2O_4$ and SiO_2-$MgAl_2O_4$, Am. Mineral. 67 (1982) 696–717.

[72] P. McMillan, B. Piriou, A. Navrotsky, A Raman spectroscopic study of glasses along the joins silica-calcium aluminate, silica-sodium aluminate, and silica-potassium aluminate, Geochem. Cosmochim. Acta 46 (1982) 2021–2037.

[73] E.A. Davis, N.F. Mott, Conduction in non-crystalline systems V. Conductivity, optical absorption and photoconductivity in amorphous semiconductors, Phil. Mag. 22 (1970) 903–922, https://doi.org/10.1080/14786437008221061.

[74] D. Souri, K. Shomalian, Band gap determination by absorption spectrum fitting method (ASF) and structural properties of different compositions of (60−x) V_2O_5–$40TeO_2$–xSb_2O_3 glasses, J. Non-Cryst. Solids 355 (2009) 1597–1601, https://doi.org/10.1016/j.jnoncrysol.2009.06.003.

[75] F. Urbach, The long-wavelength edge of photographic sensitivity and of the electronic absorption of solids, Phys. Rev. 92 (1953) 1324, https://doi.org/10.1103/PhysRev.92.1324.

[76] N. Li Dai, L. Hu, W. Chen, G. Boulon, J. Yang, S. Dai, P. Lu, Spectroscopic and fluorescence decay behaviors of Yb^{3+}-doped SiO_2–PbO–Na_2O–K_2O glass, J. Lumin. 113 (2005) 221–228, https://doi.org/10.1364/OE.25.028501.

[77] L.D. Deloach, S.A. Payne, L.L. Chase, L.K. Smith, W.L. Kway, W.F. Krupke, Evaluation of absorption and emission properties of Yb^{3+} doped crystals for laser applications, IEEE J. Quant. Electron. 24 (1993) 1179–1191, https://doi.org/10.1364/AO.45.004695.

[78] W.L. Barnes, Richard I. Laming, Eleanor J. Tarbox, P.R. Morkel, Absorption and emission cross-section of Er^{3+} -doped silica fibers, IEEE J. Quant. Electron. 27 (1991) 1003–1010.

[79] D.E. McCumber, Einstein relations connecting broadband emission and absorption spectra, Phys. Rev. 136 (1964) A954–A957, https://doi.org/10.1103/PhysRev.136.A954.

[80] P. Barua, E.H. Sekiya, K. Saito, A.J. Ikushima, Influences of Yb^{3+} ion concentration on the spectroscopic properties of silica glass, J. Non-Cryst. Solids 354 (2008) 4760–4764, https://doi.org/10.1016/j.jnoncrysol.2008.04.020.

[81] J.H. Choi, A. Margaryan, F.G. Shi, Optical transition properties of Yb^{3+} in new fluorophosphate glasses with high gain coefficient, J. Alloys Compd. 396 (2005) 79–85, https://doi.org/10.1016/j.jallcom.2004.10.076.

[82] J.H. Choi, A. Margaryan, F.G. Shi, Spectroscopic properties of Yb^{3+} in heavy metal contained fluorophosphate glasses, Mater. Res. Bull. 40 (2005) 2189–2197, https://doi.org/10.1016/j.materresbull.2005.06.015.

[83] H. Takebe, T. Murata, K. Morinaga, Compositional dependence of absorption and fluorescence of Yb^{3+} in oxide glasses, J. Am. Ceram. Soc. 79 (1996) 681–687, https://doi.org/10.1111/J.1151-2916.1996.TB07929.X.

[84] K. Venkata Krishnaiah, R. Rajeswari, K. Upendra Kumar, S. Surendra Babu, I. R. Martín, C.K. Jayasankar, Spectroscopy and radiation trapping of Yb3+ ions in lead phosphate glasses, J. Quant. Spectrosc. Radiat. Transf. 140 (2014) 37–47, https://doi.org/10.1016/j.jqsrt.2014.02.003.

[85] Q. Zhang, J. Ding, B. Tang, J. Cheng, Y. Qiao, Q. Zhou, J. Qiu, Q. Chen, D. Chen, Optical properties of Yb^{3+} ions in SiO_2-Al_2O_3-CaF_2 glasses, J. Phys. D Appl. Phys. 42 (2009) 235405-1–235405-4, https://doi.org/10.1088/0022-3727/42/23/235405.

[86] T. Forster, Intermolecular energy migration and fluorescence, Ann. Phys. 437 (1948) 55–75.

[87] D.L. Dexter, A theory of sensitized luminescence in solids, J. Chem. Phys. 21 (1953) 836–850, https://doi.org/10.1063/1.1699044.